J Mater Sci: Mater Electron **(2023) 34:1945**

Investigation on the passivation at the GeO_x/Ge interface trap with high oxidation state in GeO_x formed by ozone oxidation

Lixing Zhou[1,*] , Jialu Cui[1], Xiaolei Wang[2,3], and Shiwei Feng[1]

[1] *Faculty of Information Technology, School of Microelectronics, Beijing University of Technology, Beijing 100124, China*
[2] *Key Laboratory of Microelectronics Devices & Integrated Technology, Institute of Microelectronics of Chinese Academy of Sciences, Beijing 100029, China*
[3] *University of Chinese Academy of Sciences, Beijing 100049, China*

Received: 9 May 2023
Accepted: 13 September 2023
Published online:
5 October 2023

© The Author(s), under exclusive licence to Springer Science+Business Media, LLC, part of Springer Nature, 2023

ABSTRACT

The need to achieve low interface state density (D_{it}) at oxide/Ge interface for Ge metal–oxide–semiconductor devices promotes research into interface passivation engineering. In this paper, the D_{it} distribution with different GeO_x thicknesses and post-deposition annealing (PDA) ambient is investigated based on ozone oxidation. The results show that D_{it} at the GeO_x/Ge interface decreases with increasing GeO_x thickness. Moreover, the D_{it} slightly increases following PDA in N_2 while decreases following PDA in O_2. The X-ray photoelectron spectroscopy (XPS) is employed to investigate the distribution of Ge oxidation state (Ge^{1+}, Ge^{2+}, Ge^{3+}, and Ge^{4+}) in different GeO_x thicknesses and PDA ambient. The XPS results show that the content of Ge^{3+} oxide component increases as the GeO_x thickness increases. Compared with untreated samples, N_2 PDA induces a lower Ge^{3+} content and higher D_{it}, while O_2 PDA induces a higher Ge^{3+} content and lower D_{it}. Therefore, Ge^{3+} oxide component is responsible for the D_{it} passivation. The partial density of states obtained by first-principles calculation with $Ge^{1+}Ge^{3+}$/Ge structure shows the removal of trap state within Ge band gap compared with that of $Ge^{1+}Ge^{2+}$/Ge structure, which agrees with the experiment results. This study gives another insight into the passivation mechanism at semiconductor/oxide interface.

1 Introduction

The semiconductor/oxide interface is a basic constituent in modern electronics devices, such as metal–oxide–semiconductor field-effect transistors (MOSFETs). The semiconductor/oxide interface strongly influences various crucial electrical properties of MOSFETs, such as threshold voltage, carrier mobility, 1/f noise, radiation response, long-term reliability, and stability [1–6]. Amount of dangling bonds exit at the semiconductor/oxide interface due to the interruption of the periodic lattice structure. The dangling bonds can be charged by the gain or loss of electron. These interfacial defects induce trap energy levels in

Address correspondence to E-mail: zhoulixing@bjut.edu.cn

https://doi.org/10.1007/s10854-023-11334-5

the semiconductor band gap and play a dominant role in degrading the device performance [1]. At the crystalline-Si/amorphous-SiO_2 interface, the interfacial states are primarily Si dangling bonds or the P_b centers [1, 2, 7–10], such as the P_b for (111) and (110) Si orientations and P_{b0} and P_{b1} for (100) Si orientation [11–13]. In addition, a paramagnetic recombination center named P_m center [14] and Si_nO_{3-n}≡Si· (n = 1, 2) defect named S center [15] were reported. With further scaling of the Si MOSFET node, performance improvement becomes increasingly difficult. Ge as channel material with better hole and electron mobility than that of Si is expected to be a significant breakthrough to achieve high performance [16, 17]. Similarly, Ge dangling bonds (Ge_3≡Ge·) were reported due to the inherent mismatch between Ge and its oxide [18–22].

In general, the density of dangling bonds and interfacial states can be reduced by sufficient oxidation or terminated with another atom. For Si case, the dangling bonds can be effectively passivated with termination to H or D by annealing in hydrogen or deuterium [23–26]. For the Ge case, the interface state density (D_{it}) is still a major technical issue hindering the application of Ge-based metal–oxide–semiconductor (MOS) devices [27, 28]. Surface passivation is a critical challenge to achieve high-quality high-k stacks. Commonly used approaches include nitride [29, 30], S [31, 32], Si [33, 34], and Ge oxide passivation [35–37]. Among these methods, Ge oxide passivation shows super electrical property with the effective passivation at the Ge/GeO_x interface having low D_{it}. In recent years, there have been extensive studies on the GeO_x passivation and Ge/GeO_x interface properties. For example, Zhang et al. [38] investigated the effect of plasma post-oxidation on the MOS interface properties of Al_2O_3/GeO_x/Ge structures with different GeO_x thicknesses. Although a relationship between D_{it} and GeO_x thickness has been reported, the mechanism behind this relationship has not been elucidated. Yang et al. [39] investigated the capacitor performance of Al_2O_3/GeO_x/Ge gate stack by ozone oxidation method. But it mainly focused on the electrical property comparison between cycling ozone oxidation and single-ozone oxidation passivation. Xu et al. [40] investigated the electrical performance of HfO_2/Al_2O_3/GeO_x/Ge pMOSFET with ozone post-oxidation and plasma post-oxidation, listing the D_{it} values following the two oxidation methods but providing no detailed explanation of the results. Although there have been numerous reports on interface passivation, especially for the GeO_x/Ge system, the researches mainly focus on the electrical property of the interface and Ge MOS devices.

The low D_{it} and low equivalent oxide thickness (EOT) are the prerequisites for continued dimensional scaling of Ge MOSFETs. Owing to the relatively low permittivity of GeO_x, decreasing the GeO_x thickness is an effective method to scale down the EOT. However, D_{it} increases when the GeO_x thickness decreases. Zhang et al. [38] reported that D_{it} increases as the GeO_x thickness decreases by plasma post-oxidation. Shibayama et al. [41] attributed the dependence of D_{it} on GeO_x thickness to the amount of Ge^{3+} oxide component by plasma thermal oxidation. Ozone oxidation is considered as an effective method to obtain superior GeO_x/Ge interface at low temperature and avoid the thermal degradation of GeO_x [42]. Kuzum et al. [43] reported that D_{it} decreases with increasing GeO_x thickness owing to the Ge^{4+} oxidation component by ozone oxidation. The passivation mechanism seems to differ between plasma oxidation and ozone oxidation. Therefore, it is necessary to further clarify the passivation mechanism by ozone oxidation and observe whether the suboxide passivation is related to the oxidation method.

In this work, we investigate the D_{it} passivation mechanism of GeO_x/Ge stack by ozone oxidation. We found the D_{it} at the Ge/GeO_x interface is not be passivated by termination with another atom. The high oxidation state of GeO_x is the main reason for the decrease of D_{it}. We propose a possible physical mechanism to explain the D_{it} passivation, namely remote Coulomb potential perturbation from high oxidation state of GeO_x. This remote Coulomb potential shifts the eigen energy of dangling bonds, moving it from the band gap into the conduction or valence band and passivating D_{it}.

2 Experiment

We fabricated Ge-sub MOS capacitors and film stacks to explore the distributions of D_{it} and different Ge oxidation states, respectively. As for the capacitor samples, the GeO_x/Al_2O_3 gate stack was used. After cleaning the Ge surface in HF (100:1) for 60 s, the GeO_x was grown by ozone oxidation at 300 °C. The oxidation time was varied to control the GeO_x thickness. Then, 10 nm Al_2O_3 was deposited by atomic layer deposition (ALD) using trimethylaluminum (TMA) and H_2O

as precursors at 300 °C. After post-deposition annealing (PDA) at 400 °C in N_2 for 5 min, 30 nm TiN and 75 nm W were deposited by ALD. Al was used as the backside contact. All these samples were annealed in forming gas ambient at 400 °C for 30 min. In addition, the Ge MOS capacitors with GeO_x/Al_2O_3 gate stack were fabricated in different PDA ambients. GeO_x was grown by ozone oxidation at 300 °C for 25 min. 10 nm Al_2O_3 was then deposited at 300 °C. One sample was not annealed and used as the control. The others underwent PDA in N_2 and O_2 ambient at 400 °C for 30 min. Subsequently, the metal electrode was formed using the same process conditions as above. As for the Ge/GeO_x/Al_2O_3 film stack samples, one group was with different GeO_x thicknesses and the same thickness of Al_2O_3 of 1 nm, and the other group was with 0.7 nm GeO_x and 2 nm Al_2O_3 in different PDA ambients. The X-ray photoemission spectroscopy (XPS) measurement was performed using Thermo Scientific ESCALAB 250xi equipped with a monochromatic Al Kα radiation source of 1486.8 eV. The pass energy was set as 15 eV. All data were collected at a take-off angle of 90° relative to the sample surface.

3 Results and discussion

The electrical property of MOS capacitors with different GeO_x thicknesses is investigated. The D_{it} is measured using the low-temperature conductance method. Figure 1 shows the D_{it} at 0.3 eV above the valence band maximum vs. GeO_x thickness. D_{it} rapidly decreases as the GeO_x thickness increases up to 8 Å but varies minimally when the GeO_x thickness increases beyond 8 Å. Therefore, D_{it} at the Ge/GeO_x interface is dependent on the GeO_x thickness. These results show that ozone oxidation leads to the same D_{it} trend with GeO_x thickness as plasma oxidation [44, 45]. A GeO_x layer with thickness larger than 8 Å is necessary to achieve good electrical property. The inset in Fig. 1 shows the capacitance–voltage (*C*–*V*) curves of MOS capacitor with 10.6 Å GeO_x at multiple frequencies. Super *C*–*V* curves indicate a low D_{it} and high-quality Ge/GeO_x interface.

Studies have shown that D_{it} at the Ge/GeO_x interface correlates with Ge dangling bonds or oxygen-related defects [22, 46]. Oxygen deficiency leads to oxygen vacancies and Ge dangling bonds near the Ge/GeO_x interface [19, 47]. To investigate the origin of the D_{it}–GeO_x thickness relationship, the chemical

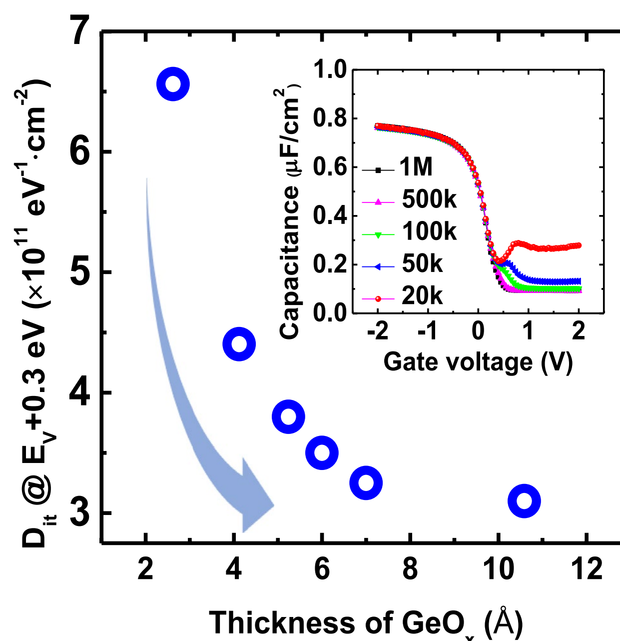

Fig. 1 D_{it} as a function of GeO_x thickness. The inset shows the *C*–*V* curves of the MOS capacitors with 10.6 Å GeO_x

state of Ge is examined using XPS. Figure 2 shows the Ge 3*d* spectra of Ge/GeO_x stacks with different GeO_x thicknesses. The Ge 3*d* peaks at binding energy of 29.35 and 32 eV are from Ge substrate and GeO_x, respectively. The peak signal corresponding to GeO_x gradually increases with a thicker GeO_x layer. The chemical shifts of Ge^{1+}, Ge^{2+}, Ge^{3+}, and Ge^{4+} relative to that of Ge^0 are taken as 0.8, 1.8, 2.75, and 3.4 eV, respectively [48, 49]. The full widths at half maximum (FWHM) for Ge^0, Ge^{1+}, Ge^{2+}, Ge^{3+}, and Ge^{4+} spectra are determined to be 0.57, 0.57, 0.9, 1.12, and 1.2 eV, respectively. Each core-level spectrum was fitted by a nonlinear Gaussian–Lorentzian line shape and Shirley background subtraction. The fixed spin orbit splitting of Ge 3d is 0.58 eV. Figure 2(a) shows the Ge 3*d* spectrum of the 4.1 Å GeO_x. Only Ge^{1+} and Ge^{2+} signals are observed, and no Ge^{3+} and Ge^{4+} signals are detected. For the 6.6 Å GeO_x, Ge^{3+} signal is obvious but Ge^{4+} signal is extremely small as shown in Fig. 2b. Figure 2c shows Ge^{3+} and Ge^{4+} signals become more evident in a thicker GeO_x of 7.8 Å. In addition, we analyze the Ge(GeO_x) to O(GeO_x) areal intensity ratio as a function of GeO_x thickness, as shown in Fig. 3. The value of Ge(GeO_x)/O(GeO_x) decreases with increasing GeO_x thickness, which suggests that the oxygen content in GeO_x is comparatively low in a thinner GeO_x and increases as

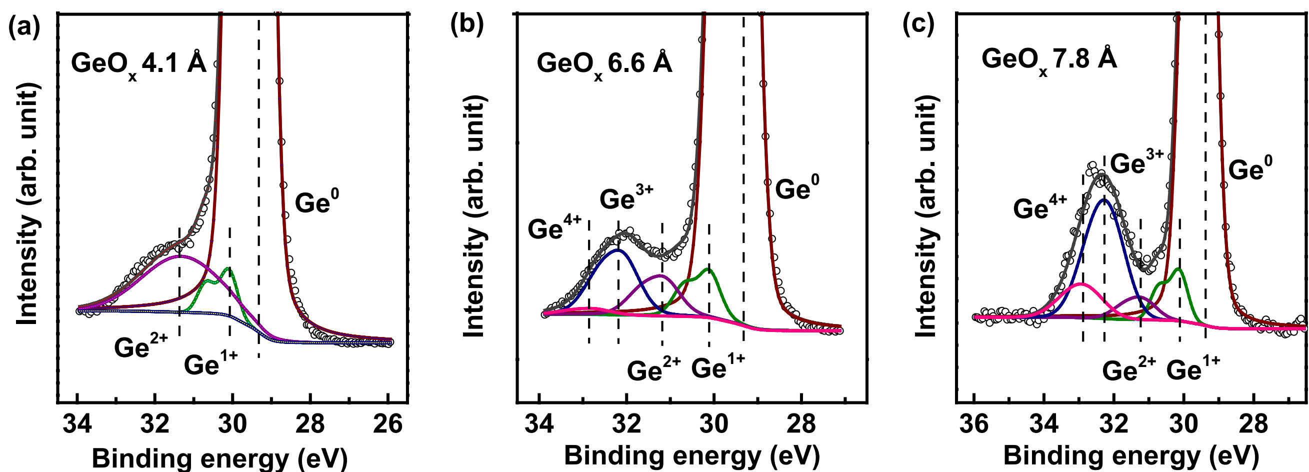

Fig. 2 Ge 3*d* spectra of Ge/GeO_x stack with GeO_x thickness of **a** 4.1 Å, **b** 6.6 Å, and **c** 7.8 Å

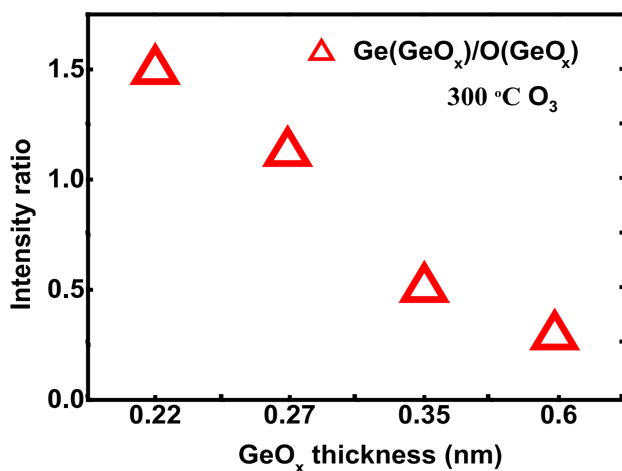

Fig. 3 The areal intensity ratio of Ge(GeO_x) vs. O(GeO_x) for different GeO_x thicknesses

the GeO_x thickness increases. Oxygen is relevantly deficient, and it results in the Ge dangling bonds the Ge/GeO_x interface.

The composition changes of each chemical state, namely Ge^{1+}, Ge^{2+}, Ge^{3+}, and Ge^{4+}, is quantitatively calculated, as shown in Fig. 4a–d. The Ge^{1+} content is unaffected by the GeO_x thickness. The Ge^{2+} content increases initially and then is unchanged when the GeO_x thickness increases beyond after 4.1 Å. The Ge^{3+} content increases with increasing GeO_x thickness. The Ge^{4+} signal is undetectable when the GeO_x thickness is less than 8 Å and increases markedly when the GeO_x thickness increases beyond 8 Å. The shaded area covering the GeO_x thickness from 2 to 8 Å is the region of D_{it} reduction. D_{it} remains unchanged when the GeO_x thickness is greater than 8 Å, as shown in Fig. 1.

We discuss the microstructure and chemical bonding states near the Ge/GeO_x interface based on the above XPS results. Owning to the mismatch of Ge substrate and GeO_x, the low oxidation states locate near the Ge substrate at the Ge/GeO_x interface. The Ge^{1+} and Ge^{2+} states are localized mainly in the first and second Ge oxidation layers. This conclusion can be further confirmed as follows. The Ge^{1+} and Ge^{2+} signals are nearly unchanged when the GeO_x thickness is greater than 4.1 Å, as shown in Fig. 4a, b. This value of 4.1 Å corresponds to oxidation of two Ge layers, which is explained as follows. The distance between Ge and O atom layers in GeO_x (here we denote it as Ge–O) is ~ 1–1.6 Å [50, 51]. Thus, the GeO_x thickness corresponding to the oxidation of two Ge layers, i.e., Ge–O–Ge–O, is ~ (1–1.6) × 3= ~ (3–4.8) Å. This value is consistent with the value of ~ 4.1 Å. As shown in Fig. 2a, the 4.1 Å GeO_x only contains Ge^{1+} and Ge^{2+} states. Consequently, the Ge^{1+} and Ge^{2+} states are localized mainly in the first and second Ge oxidation layers. Moreover, the interfacial oxidation state and microstructure at the Ge/GeO_x interface can be considered unchanged when GeO_x thickness is beyond 4.1 Å, i.e., the distribution of Ge dangling bonds at the Ge/GeO_x interface is unchanged during the process of ozone oxidation. While the D_{it} keeps to decrease when GeO_x thickness is greater than 4.1 Å. These results suggest that the decrease of D_{it} at the Ge/GeO_x interface does not arise from the passivation of Ge dangling bonds

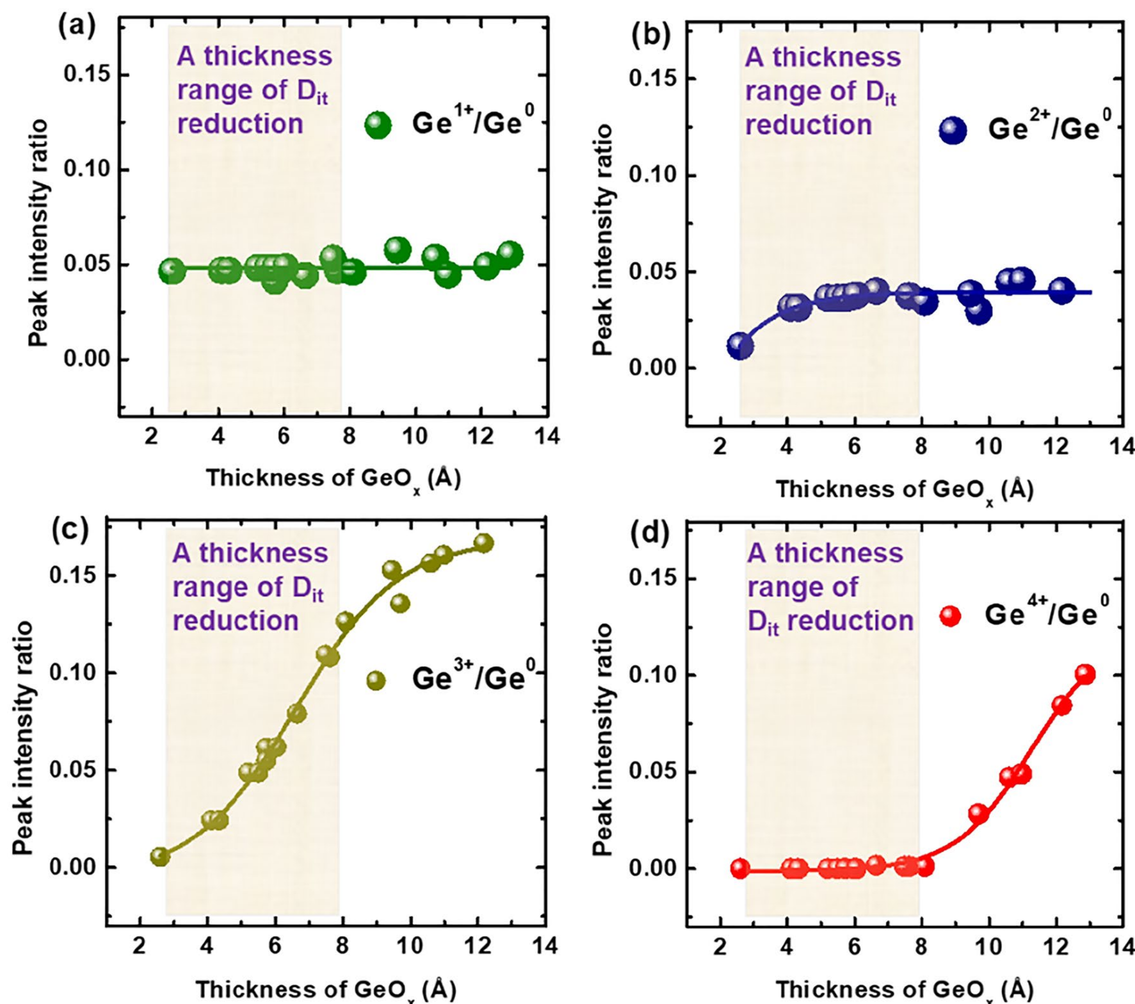

Fig. 4 Areal intensity of Ge chemical state of **a** Ge^{1+}, **b** Ge^{2+}, **c** Ge^{3+}, and **d** Ge^{4+} with GeO_x thickness. The shaded area is the region of D_{it} reduction

by additional oxygen atoms. D_{it} continues to decrease and the Ge^{3+} content keeps to increase as the GeO_x thickness increases from 2 to 8 Å in Figs. 1 and 2. The relationship between D_{it} and the content ratio of Ge^{3+} in GeO_x and Ge^0 in Ge substrate is shown in Fig. 5. D_{it} decreases with increasing Ge^{3+} content, which means Ge^{3+} plays an important role in D_{it} passivation by ozone oxidation. Similar results have been reported for plasma oxidation [41]. Both for plasma and ozone oxidation, D_{it} similarly changes with increasing GeO_x thickness. Therefore, Ge^{3+} plays a key role in the D_{it} passivation at the GeO_x/Ge interface regardless of the oxidation method.

One can propose another possible reason that is the mechanical stress exerted by different thicknesses of GeO_x to induce D_{it} passivation. However, D_{it} decreases

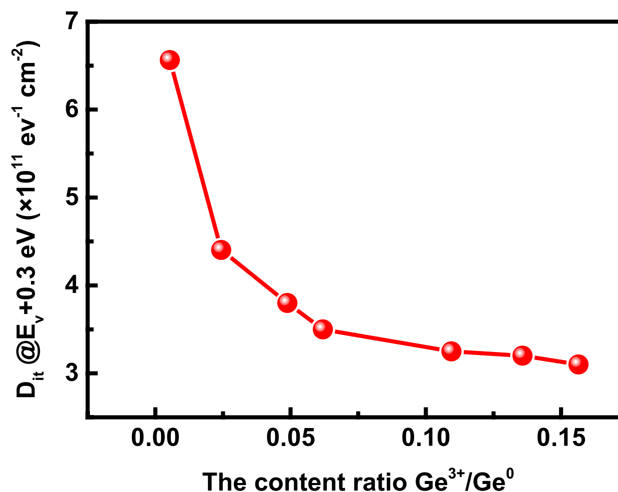

Fig. 5 D_{it} as a function of the content ratio of Ge^{3+} in GeO_x and Ge^0 in Ge substrate

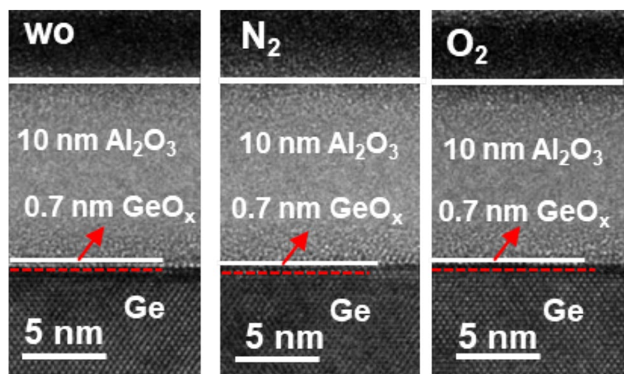

Fig. 6 HRTEM images of the GeO_x/Al_2O_3 structures without PDA and with PDA in N_2 and O_2 ambient

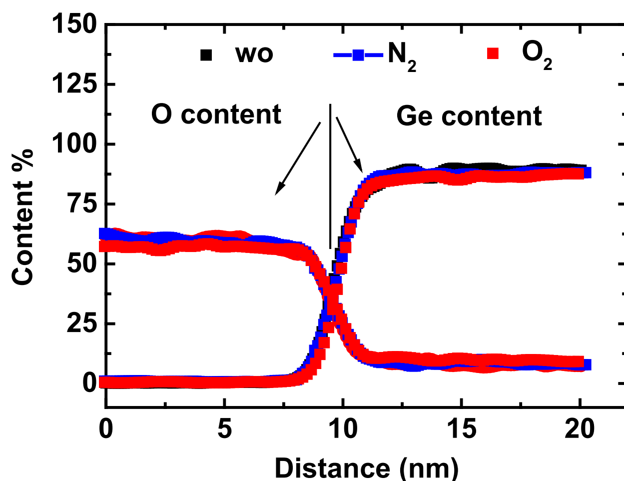

Fig. 7 EDS depth profiles for $Ge/GeO_x/Al_2O_3$ structures without PDA and with PDA in N_2 and O_2 ambient

when GeO_x thickness is less than 8 Å and is unchanged when GeO_x thickness is larger than 8 Å, as shown in Fig. 1. Moreover, the Ge^{3+} content increases as the GeO_x thickness increases from 2 to 8 Å and gradually stabilizes as the GeO_x thickness is larger than 8 Å. While the stress at the GeO_x/Ge interface still increases when GeO_x thickness is larger than 8 Å. This is inconsistent with the change in D_{it}. To further investigate the effect of stress on D_{it}, the samples were treated in different PDA ambients to observe the changes of the gate stack and D_{it}. Figure 6 shows the high-resolution transmission electron microscope (HRTEM) images of the GeO_x/Al_2O_3 structure without PDA and with PDA in N_2 and O_2 ambient. The thickness of the GeO_x interlayer is nearly unchanged after PDA. The stress at the Ge/GeO_x interface is also considered the same for different PDA samples. Figure 7 shows the energy-dispersive spectroscopy (EDS) depth profiles of Ge and O elements for $Ge/GeO_x/Al_2O_3$ structure without PDA and with PDA in N_2 and O_2. PDA does not change the physical thickness of the gate dielectrics. The EDS results show that the depth profiles of the O and Ge elements are the same after PDA, indicating that the physical structure does not change. Therefore, the change in D_{it} does not arise from the physical structure or elemental interdiffusion during N_2 and O_2 PDA.

Figure 8 shows the *C*–*V* characteristics of Ge MOS capacitors at multiple frequencies and the D_{it} for various PDA ambients. Well *C*–*V* plot indicates good interface quality. The D_{it} was obtained by the low-temperature conductance method. As shown in Fig. 8d, D_{it} slightly differs depending on the PDA treatment: without PDA, N_2 PDA, and O_2 PDA. O_2 PDA is more beneficial for the D_{it} passivation than N_2 PDA and without PDA condition. Although the GeO_x thickness does not change, D_{it} distribution shows slight difference between the N_2 and O_2 PDA-treated samples. Therefore, the mechanical stress exerted by different thicknesses of GeO_x as the origin of the D_{it} variation is excluded. D_{it} reduction at the Ge/GeO_x interface does not arise from the passivation of dangling bonds by another atom or the stress from the different thicknesses of GeO_x, but from the appearance of high Ge oxidation states. The contribution of high Ge oxidation state in GeO_x to D_{it} reduction has been observed in other studies in which the GeO_x was grown by H_2O plasma oxidation in an ALD chamber [52]. A longer deposition time enhances the Ge oxidation state, which decreases the D_{it}.

Figure 9 provides the XPS Ge 3d spectra of $Ge/GeO_x/Al_2O_3$ in different PDA ambients. The corresponding intensity ratio of Ge^{1+}, Ge^{2+}, Ge^{3+}, and Ge^{4+} in GeO_x is shown in Fig. 10. The results show that the Ge^{3+} component in GeO_x increases after O_2 PDA while decreases after N_2 PDA. Ge^{1+} component in GeO_x has nearly no changes after PDA, indicating that the PDA has a negligible effect on Ge dangling bonds. Although the amount of Ge dangling bonds is similar, D_{it} still shows different distribution in N_2 and O_2 PDA as shown in Fig. 8d. The Ge^{2+} component in GeO_x is similar between N_2 and O_2 PDA sample, indicating that Ge^{2+} is not the main sources of D_{it} passivation. The content of Ge^{4+} component decreases after PDA in N_2 and O_2 compared with the untreated sample. This changes of Ge^{4+} content after PDA is inconsistent with that of D_{it}. While the Ge^{3+} component in GeO_x

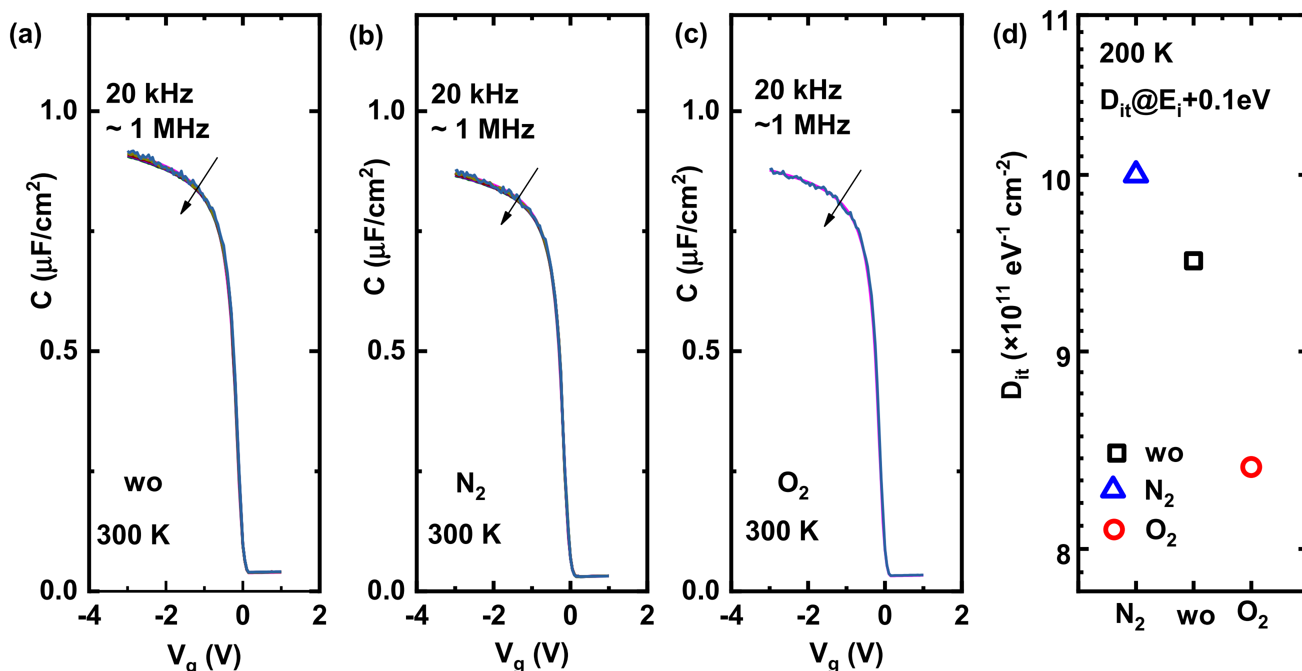

Fig. 8 C–V plots of Ge MOS capacitors with GeO_x/Al_2O_3 gate stack in different PDA ambients: **a** without PDA, **b** N_2 and **c** O_2. **d** D_{it} for different PDA ambients

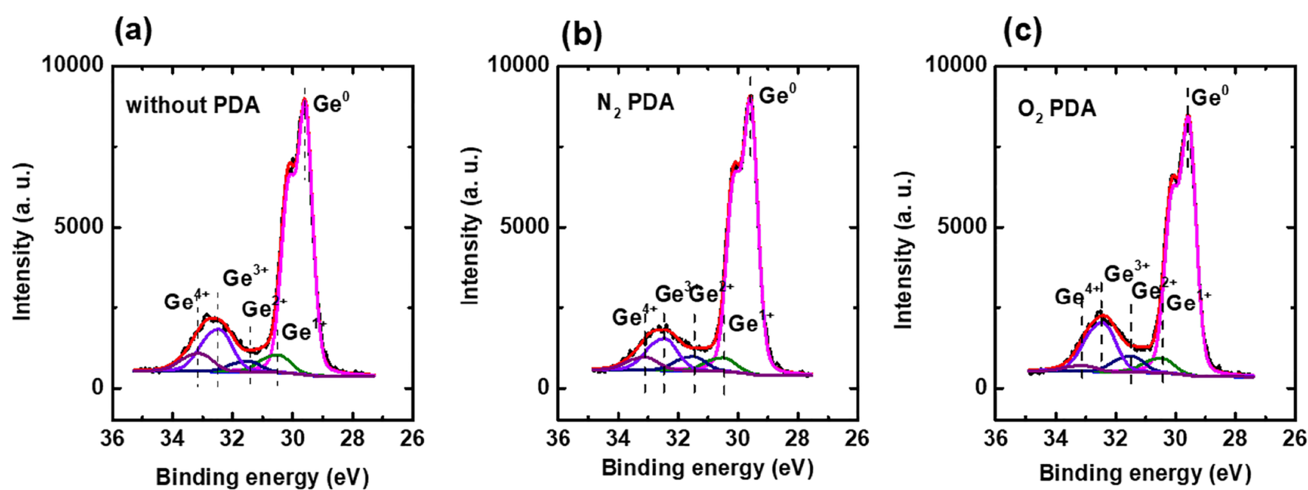

Fig. 9 Ge 3d spectra of Ge/GeO_x stacks **a** without PDA, **b** with N_2 PDA, and **c** with O_2 PDA

increases after O_2 PDA and decreases after N_2 PDA, which declares Ge^{3+} is responsible for the D_{it} passivation. The change of D_{it} distribution is related to the content of Ge^{3+} oxidation state component. This is consistent with the result for D_{it} dependence on GeO_x thickness. D_{it} only decreases at the GeO_x thickness range of 2 ~ 8 Å but remains unchanged with GeO_x thickness larger than 8 Å. Moreover, the content of Ge^{3+} component obviously increases as the GeO_x thickness increases from 2 to 8 Å, and gradually stabilizes as the GeO_x thickness increases beyond 8 Å. These results demonstrate that the Ge^{3+} component is responsible for the D_{it} passivation.

To examine the above experimental results, we employed first-principles modeling to observe the remote passivation effect of Ge^{3+} on the gap state. The

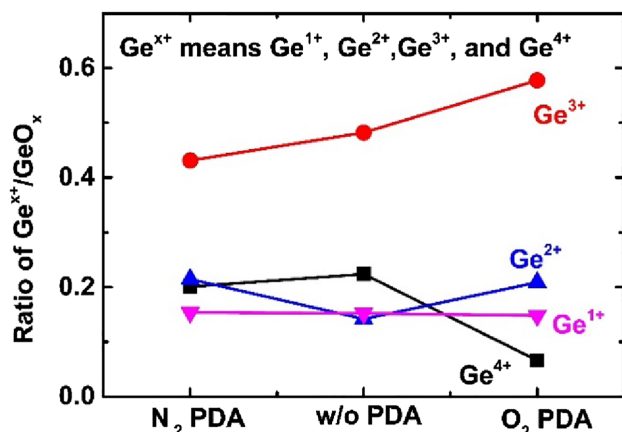

Fig. 10 The intensity ratio of Ge^{1+}, Ge^{2+}, Ge^{3+}, and Ge^{4+} in GeO_x for the without PDA, and with N_2 and O_2 PDA samples

calculations were performed within density functional theory, as implemented in the code Vienna ab initio simulation package [53]. The projector augmented plane-wave method with Perdew–Burke–Ernzerhof was used [54]. The generalized gradient approximation was constructed for the exchange-correlation potential. A plane wave with 450 eV cut-off energy was used for the structural relaxation. All the structures were relaxed until the residual forces on the atoms declined to less than 0.02 eV/Å. The energy criterion in the iterative solution of the Kohn–Sham equation was set to be 10^{-5} eV. The interface region was modeled in a 20 Å vacuum spacing perpendicular to the slab to avoid interlaminar interactions. In this study, we mainly consider the changes of partial density of states (PDOS) by the introduction of Ge^{3+}.

Figure 11a shows the atomic structure of GeO_x with Ge^{1+} and Ge^{2+} at the Ge/GeO_x interface and corresponding PDOS. The results show that Ge^{1+} induces defect states within the Ge band gap, while Ge^{2+} leaves no gap states within the Ge band gap. This means Ge^{1+}, without oxidated sufficiently, at Ge/GeO_x interface plays a key role in the D_{it}. Ge^{2+} has little effect on

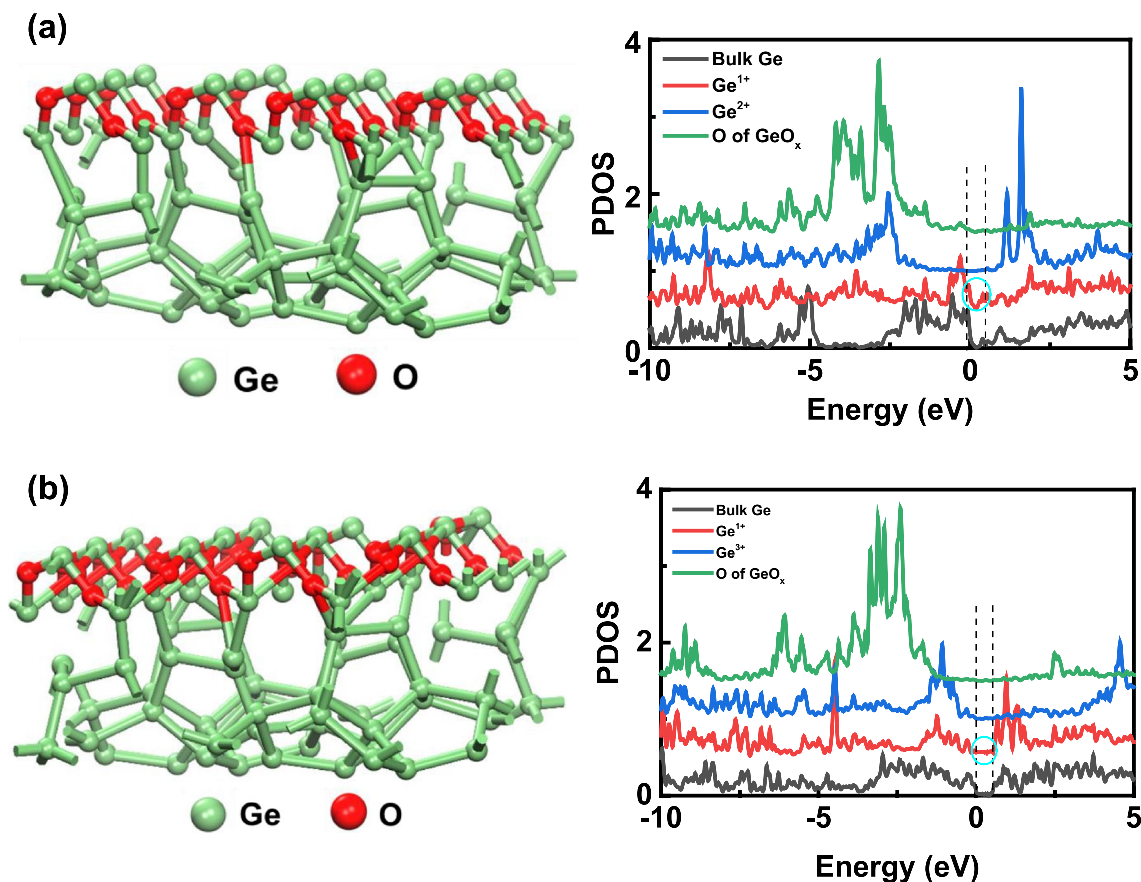

Fig. 11 **a** Atomic structure of GeO_x with Ge^{1+} and Ge^{2+} and PDOS at the Ge/GeO_x interface. **b** Atomic structure of GeO_x with Ge^{1+} and Ge^{3+} and PDOS at the Ge/GeO_x interface

the D_{it}. In contrast, Ge^{3+} has the effect of removing the trap states of Ge^{1+} from the band gap energy range, as illustrated in Fig. 11b. The calculation result is consistent with the experimental result in that the Ge^{3+} reduces the trap states at the Ge/GeO_x interface. In the study of investigating the dependence of D_{it} on GeO_x thickness, D_{it} reduces as the GeO_x thickness increases up to 8 Å. In this range of GeO_x thickness, the Ge^{3+} content markedly increases, which passivates the trap states and reduces D_{it} at the Ge/GeO_x interface. When GeO_x thickness is larger than 8 Å, the Ge^{3+} content gradually saturates and D_{it} drops to a minimum and remains unchanged.

We discuss a possible physical origin of D_{it} decrease at the Ge/GeO_x interface by ozone oxidation. We consider the remote Coulomb potential perturbation from high oxidation state Ge atoms, based on the perturbation theory of quantum mechanisms. In general, the D_{it} originates from dangling bonds [19, 22], as shown in Fig. 12a, c. The appearance of additional Ge atoms with higher oxidation states induces a remote Coulomb potential near the dangling bonds, as show in Fig. 12b. This Coulomb potential perturbation can induce an eigen energy shift of the dangling bond based on the perturbation theory of quantum mechanisms, as shown in Fig. 12c. If this shift moves the eigen energy of the dangling bonds from the band gap into the valence band, then D_{it} is passivated. It should be noted that the dangling bond is passivated by the eigen energy shift into valence band induced by remote Coulomb charges, such as Ge^{3+}, not by termination with another atom. The D_{it} passivation by Ge high oxidation state is verified by analyzing the samples produced under different thickness GeO_x and different PDA ambient conditions. The GeO_x thickness and PDA ambient affects the distribution of Ge^{3+} oxidation state in GeO_x, which induces corresponding D_{it} variation. The perturbation theory of quantum mechanisms is a possibly reasonable explanation for D_{it} passivation.

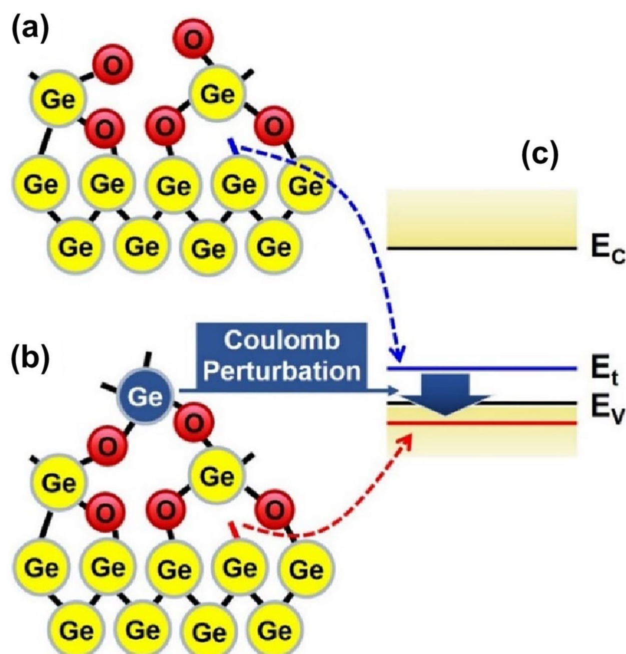

Fig. 12 Schematic of the D_{it} passivation mechanism of remote Coulomb perturbation. A dangling bond of the Ge substrate (**a**) induces the interfacial trap eigen energy in the Ge band gap (**c**). The appearance of the Ge atom with high oxidation state (**b**) induces a remote Coulomb potential perturbation near the dangling bond, shifting the eigen energy of the interfacial trap. This energy shift moves the interfacial trap from the band gap into the valence band, consequently passivating the D_{it}

4 Conclusion

In this study, passivation of the Ge/GeO_x interface by ozone oxidation is investigated, and a possible passivation mechanism is proposed. The experimental results indicate that the D_{it} passivation is related to the Ge^{3+} oxidation state in GeO_x. D_{it} at the Ge/GeO_x interface dramatically decreases and the Ge^{3+} content constantly increased as the GeO_x thickness increased up to 8 Å. The effect of Ge^{3+} oxidation state is also demonstrated by different PDA ambients. The Ge^{3+} content differs after PDA and leads to different D_{it} distribution. The PDOS obtained by first-principles calculation with Ge^{3+} component in GeO_x shows the removal of trap state from the band gap, which is in good agreement with the experiment results. The high Ge oxidation states may induce a remote Coulomb potential to move the dangling bond eigen energy from the band gap into the conduction or valance band to passivate D_{it}. This study provides another insight into the passivation mechanism at the semiconductor/oxide interface.

Author contributions

LZ wrote and revised the article. JC performed material and sample preparation. XW carried out the data characterization. SF anchored the review and

revisions. All the authors read and approved the final manuscript.

Funding

This work is supported by the National Natural Science Foundation of China (No. 62204009) and the Scientific Research Common Program of Beijing Municipal Commission of Education (No. KM202210005024).

Data availability

The datasets generated during and/or analyzed during the current study are available from the corresponding author on reasonable request.

Declarations

Conflict of interest There are no conflicts to declare.

References

1. E. Mehes, C. Patterson, Defects at the Si (001)/a–SiO_2 interface: analysis of structures generated with classical force fields and density functional theory. Phys. Rev. Mater. **1**(4), 044602 (2017)
2. K. Keunen, A. Stesmans, V. Afanas'ev, Inherent Si dangling bond defects at the thermal (110) Si/SiO_2 interface. Phys. Rev. B **84**(8), 085329 (2011)
3. A. Rakoski, S. Diez, H. Li, S. Keller, E. Ahmadi, Ã. Kurdak, Electron transport in N-polar GaN-based heterostructures. Appl. Phys. Lett. **114**(16), 162102 (2019)
4. S.K. Kim, D.-M. Geum, J.-P. Shim, C.Z. Kim, H.-. Kim, J.D. Song, W.J. Choi, S.-J. Choi, D.H. Kim, S. Kim, Fabrication and characterization of Pt/Al_2O_3/Y_2O_3/$In_{0.53}Ga_{0.47}As$ MOSFETs with low interface trap density. Appl. Phys. Lett. **110**(4), 043501 (2017)
5. A. Jayawardena, R.P. Ramamurthy, A.C. Ahyi, D. Morisette, S. Dhar, Interface trapping in (2^{-} 01) β-Ga_2O_3 MOS capacitors with deposited dielectrics. Appl. Phys. Lett. **112**(19), 192108 (2018)
6. X.-F. Zheng, S.-S. Dong, P. Ji, C. Wang, Y.-L. He, L. Lv, X.-H. Ma, Y. Hao, Characterization of bulk traps and interface states in AlGaN/GaN heterostructure under proton irradiation. Appl. Phys. Lett. **112**(23), 233504 (2018)
7. H. Von Bardeleben, J. Cantin, EPR Studies of the microscopic structure of the (100) Si/SiO_2 interface: current status and perspectives. Braz. J. Phys. **27**(2), 314–324 (1997)
8. A. Stesmans, B. Nouwen, V. Afanas'ev, P_{b1} interface defect in thermal (100) Si/SiO_2: ^{29}Si hyperfine interaction. Phys. Rev. B **58**(23), 15801 (1998)
9. A. Stesmans, E.V. Afanas, Undetectability of the point defect as an interface state in thermal. J. Phys. **10**(1), L19 (1998)
10. P. Lenahan, J. Conley Jr., What can electron paramagnetic resonance tell us about the Si/SiO_2 system? J. Vac. Sci. Technol. B **16**(4), 2134–2153 (1998)
11. E.H. Poindexter, P.J. Caplan, B.E. Deal, R.R. Razouk, Interface states and electron spin resonance centers in thermally oxidized (111) and (100) silicon wafers. J. Appl. Phys. **52**(2), 879–884 (1981)
12. C.R. Helms, E.H. Poindexter, The silicon-silicon dioxide system: its microstructure and imperfections. Rep. Prog. Phys. **57**(8), 791 (1994)
13. M. Jivanescu, A. Stesmans, M. Zacharias, Inherent paramagnetic defects in layered Si/SiO_2 superstructures with Si nanocrystals. J. Appl. Phys. **104**(10), 103518 (2008)
14. T. Matsuoka, L. Vlasenko, M. Vlasenko, T. Sekiguchi, K.M. Itoh, Identification of a paramagnetic recombination center in silicon/silicon-dioxide interface. Appl. Phys. Lett. **100**(15), 152107 (2012)
15. A. Stesmans, B. Nouwen, V. Afanas'ev, Structural degradation of thermal SiO_2 on Si by high-temperature annealing: defect generation. Phys. Rev. B **66**(4), 045307 (2002)
16. S. Takagi, R. Zhang, J. Suh, S.-H. Kim, M. Yokoyama, K. Nishi, M. Takenaka, III–V/Ge channel MOS device technologies in nano CMOS era. Jpn. J. Appl. Phys. **54**(6S1), 06FA01 (2015)
17. Y. Li, R. Zhang, Hole mobility in the ultra-thin-body junctionless germanium-on-insulator p-channel metal-oxide-semiconductor field-effect transistors. Appl. Phys. Lett. **114**(13), 132101 (2019)
18. J.R. Weber, A. Janotti, P. Rinke, C. Van de Walle, Dangling-bond defects and hydrogen passivation in germanium. Appl. Phys. Lett. **91**(14), 142101 (2007)
19. M. Houssa, G. Pourtois, M. Caymax, M. Meuris, M. Heyns, V. Afanas' Ev, A. Stesmans, Ge dangling bonds at the (100) Ge/GeO_2 interface and the viscoelastic properties of GeO_2. Appl. Phys. Lett. **93**(16), 161909 (2008)
20. P. Broqvist, A. Alkauskas, A. Pasquarello, Charge transition levels of the Ge dangling bond defect at Ge/insulator interfaces. Mater. Sci. Semiconduct. Process. **11**(5–6), 226–229 (2008)

21. P. Broqvist, A. Alkauskas, A. Pasquarello, Defect levels of dangling bonds in silicon and germanium through hybrid functionals. Phys. Rev. B **78**(7), 075203 (2008)
22. S. Baldovino, A. Molle, M. Fanciulli, Influence of the oxidizing species on the Ge dangling bonds at the (100) Ge/GeO_2 interface. Appl. Phys. Lett. **96**(22), 222110 (2010)
23. A. Stesmans, V. Afanas'ev, Electrical activity of interfacial paramagnetic defects in thermal (100) Si/SiO_2. Phys. Rev. B **57**(16), 10030 (1998)
24. E. Nicollian, C. Berglund, P. Schmidt, J. Andrews, Electrochemical charging of thermal SiO_2 films by injected electron currents. J. Appl. Phys. **42**(13), 5654–5664 (1971)
25. D.J. DiMaria, D. Arnold, E. Cartier, Degradation and breakdown of silicon dioxide films on silicon. Appl. Phys. Lett. **61**(19), 2329–2331 (1992)
26. A. Stesmans, G. Van Gorp, Observation of dipolar interactions between P_{b0} defects at the (111) Si/SiO_2 interface. Phys. Rev. B **42**(6), 3765 (1990)
27. S. Takagi, T. Maeda, N. Taoka, M. Nishizawa, Y. Morita, K. Ikeda, Y. Yamashita, M. Nishikawa, H. Kumagai, R. Nakane, Gate dielectric formation and MIS interface characterization on Ge. Microelectron. Eng. **84**(9–10), 2314–2319 (2007)
28. A. Toriumi, T. Tabata, C.H. Lee, T. Nishimura, K. Kita, K. Nagashio, Opportunities and challenges for Ge CMOS–Control of interfacing field on Ge is a key. Microelectron. Eng. **86**(7–9), 1571–1576 (2009)
29. K. Kutsuki, G. Okamoto, T. Hosoi, T. Shimura, H. Watanabe, Germanium oxynitride gate dielectrics formed by plasma nitridation of ultrathin thermal oxides on Ge (100). Appl. Phys. Lett. **95**(2), 022102 (2009)
30. Y. Otani, Y. Itayama, T. Tanaka, Y. Fukuda, H. Toyota, T. Ono, M. Mitsui, K. Nakagawa, Fabrication of Ta_2O_5/GeN_x gate insulator stack for Ge metal-insulator-semiconductor structures by electron-cyclotron-resonance plasma nitridation and sputtering deposition techniques. Appl. Phys. Lett. **90**(14), 142114 (2007)
31. M. Houssa, D. Nelis, D. Hellin, G. Pourtois, T. Conard, K. Paredis, K. Vanormelingen, A. Vantomme, M. Van Bael, J. Mullens, H_2S exposure of a (100) Ge surface: Evidences for a (2×1) electrically passivated surface. Appl. Phys. Lett. **90**(22), 222105 (2007)
32. R. Xie, C. Zhu, Effects of sulfur passivation on germanium MOS capacitors with HfON gate dielectric. IEEE Electron Device Lett. **28**(11), 976–979 (2007)
33. R. Pillarisetty, B. Chu-Kung, S. Corcoran, G. Dewey, J. Kavalieros, H. Kennel, R. Kotlyar, V. Le, D. Lionberger, M. Metz, High mobility strained germanium quantum well field effect transistor as the p-channel device option for low power (vcc = 0.5 V) III–V CMOS architecture. In IEEE Int. Electron Devices Meet. (IEDM) 6.7.1–6.7.4 (2010)
34. W.B. Chen, A. Chin, High performance of Ge nMOSFETs using SiO_2 interfacial layer and TiLaO gate dielectric. IEEE Electron Device Lett. **31**(1), 80–82 (2010)
35. C.H. Lee, T. Nishimura, K. Nagashio, K. Kita, A. Toriumi, High-electron-mobility Ge/GeO_2 n-MOSFETs with two-step oxidation. IEEE Trans. Electron. Devices **58**(5), 1295–1301 (2011)
36. A. Delabie, A. Alian, F. Bellenger, M. Caymax, T. Conard, A. Franquet, S. Sioncke, S. Van Elshocht, M. Heyns, M. Meuris, H_2O-and O_3-based atomic layer deposition of high-k dielectric films on GeO_2 passivation layers. J. Electrochem. Soc. **156**(10), G163–G167 (2009)
37. Q. Xie, S. Deng, M. Schaekers, D. Lin, M. Caymax, A. Delabie, Y. Jiang, X. Qu, D. Deduytsche, C. Detavernier, High-performance Ge MOS Capacitors by O_2 plasma passivation and O_2 ambient annealing. IEEE Electron Device Lett. **32**(12), 1656–1658 (2011)
38. R. Zhang, T. Iwasaki, N. Taoka, M. Takenaka, S. Takagi, Impact of GeO_x interfacial layer thickness on Al_2O_3/Ge MOS interface properties. Microelectron. Eng. **88**(7), 1533–1536 (2011)
39. X. Yang, S.-K. Wang, X. Zhang, B. Sun, W. Zhao, H.-D. Chang, Z.-H. Zeng, H. Liu, Al_2O_3/GeO_x gate stack on germanium substrate fabricated by in situ cycling ozone oxidation method. Appl. Phys. Lett. **105**(9), 092101 (2014)
40. Y. Xu, G. Han, H. Liu, Y. Wang, Y. Liu, J. Ao, Y. Hao, Ge pMOSFETs with GeO_x Passivation formed by ozone and plasma post oxidation. Nanoscale Res. Lett. **14**(1), 126 (2019)
41. S. Shibayama, K. Kato, M. Sakashita, W. Takeuchi, N. Taoka, O. Nakatsuka, S. Zaima, Impacts of AlGeO formation by post thermal oxidation of Al_2O_3/Ge structure on interfacial properties. Thin Solid Films. **557**, 282–287 (2014)
42. S.K. Wang, K. Kita, C.H. Lee, T. Tabata, T. Nishimura, K. Nagashio, A. Toriumi, Desorption kinetics of GeO from GeO_2/Ge structure. J. Appl. Phys. **108**, 054104 (2010)
43. D. Kuzum, T. Krishnamohan, A.J. Pethe, A.K. Okyay, Y. Oshima, Y. Sun, J.P. McVittie, P.A. Pianetta, P.C. McIntyre, K.C. Saraswat, Ge-interface engineering with ozone oxidation for low interface-state density. IEEE Electron Device Lett. **29**(4), 328–330 (2008)
44. R. Zhang, N. Taoka, P.-C. Huang, M. Takenaka, S. Takagi, 1-nm-thick EOT high mobility Ge n-and p-MOSFETs with ultrathin GeO_x/Ge MOS interfaces fabricated by plasma post oxidation. In IEEE Int. Electron Devices Meet. (IEDM) 28.3.1–28.3.4 (2011)

45. R. Zhang, T. Iwasaki, N. Taoka, M. Takenaka, S. Takagi, High-mobility Ge pMOSFET with 1-nm EOT Al_2O_3/GeO_x/Ge gate stack fabricated by plasma post oxidation. IEEE Trans. Electron. Devices **59**(2), 335–341 (2012)
46. L. Zhang, H. Li, Y. Guo, K. Tang, J. Woicik, J. Robertson, P.C. McIntyre, Selective passivation of GeO_2/Ge interface defects in atomic layer deposited high-k MOS structures. ACS Appl. Mater. Lnterfaces. **7**(37), 20499–20506 (2015)
47. J. Zhou, G. Han, Y. Peng, Y. Liu, J. Zhang, Q.-Q. Sun, D.W. Zhang, Y. Hao, Ferroelectric negative capacitance GeSn PFETs with Sub-20 mV/decade subthreshold swing. IEEE Electron Device Lett. **38**(8), 1157–1160 (2017)
48. D. Schmeisser, R.D. Schnell, A. Bogen, F.J. Himpsel, D. Rieger, G. Landgren, J.F. Morar, Surface oxidation states of germanium. Surf. Sci. **172**(2), 455–465 (1986)
49. S. Sun, Y. Sun, Z. Liu, D.-I. Lee, P. Pianetta, Roles of oxygen and water vapor in the oxidation of halogen terminated Ge (111) surfaces. Appl. Phys. Lett. **89**(23), 231925 (2006)
50. K. Kato, S. Kyogoku, M. Sakashita, W. Takeuchi, H. Kondo, S. Takeuchi, O. Nakatsuka, S. Zaima, Control of interfacial properties of Al_2O_3/Ge gate stack structure using radical nitridation technique. Jpn. J. Appl. Phys. **50**(10S), 10PE02 (2011)
51. G.S. Smith, P.B. Isaacs, The crystal structure of quartz-like GeO_2. Acta Crystallogr. A **17**(7), 842–846 (1964)
52. L. Chen-Chien, C.-L. Kuei-Shu, L. Li-Jung, L. Tzu-Min, F. Chung-Hao, C. Ting-Ching, C. Jen-Wei, L. Chun-Chang, W. Tien-Ko, Improved electrical characteristics of Ge MOS devices with high oxidation state in $HfGeO_x$ interfacial layer formed by in situ desorption. IEEE Electron Device Lett. **35**(5), 509–511 (2014)
53. G. Kresse, D. Joubert, From ultrasoft pseudopotentials to the projector augmented-wave method. Phys. Rev. B **59**(3), 1758–1177 (1999)
54. J.P. Perdew, K. Burke, M. Ernzerhof, Generalized gradient approximation made simple. Phys. Rev. Lett. **77**(18), 3865–3868 (1996)

Publisher's Note Springer Nature remains neutral with regard to jurisdictional claims in published maps and institutional affiliations.

Springer Nature or its licensor (e.g. a society or other partner) holds exclusive rights to this article under a publishing agreement with the author(s) or other rightsholder(s); author self-archiving of the accepted manuscript version of this article is solely governed by the terms of such publishing agreement and applicable law.